JOURNAL OF THERMOPHYSICS AND HEAT TRANSFER
Vol. 25, No. 2, April–June 2011

Diode Laser Absorption Sensor Design and Qualification for CO_2 Hypersonic Flows

Jason M. Meyers* and Doug Fletcher†
von Kármán Institute for Fluid Dynamics, 1640 Rhode Saint Genèse, Belgium

DOI: 10.2514/1.49270

The design of a diode laser absorption spectroscopy sensor to probe freestream conditions of hypervelocity CO_2 flow in the Longshot Free-Piston Facility is presented. The Longshot Facility of the von Kármán Institute is an important facility for ground test and numerical validation applications as it can produce high Mach number and high Reynold's number conditions for both N_2 and CO_2 flows. Currently, freestream conditions are determined from measurements of reservoir pressure, pitot pressure, and stagnation-point heat transfer to a hemisphere using a thermodynamic model for the expanding test gas. A nonintrusive absorption sensor can provide a direct measurement of freestream gas dynamic variables, which could be used to evaluate the data reduction process. Detailed descriptions of the design, analysis, and development of the diode laser absorption sensor are presented.

I. Introduction

LASER-SPECTROSCOPIC techniques allow access to flow parameters that are not easily measured using traditional measurements. Their ability to provide stream conditions without recourse to numerical modeling is very useful in the field of hypersonic ground testing. The knowledge gained from these nonintrusive approaches helps to improve the accuracy of both experimental data and numerical tools that can be used to further exploit physical data. Some of the more common spectroscopic measurement approaches include emission, laser induced fluorescence (LIF), two-photon absorption LIF (TALIF), and diode laser absorption spectroscopy (DLAS), which is the focus of this work.

The breadth of measurement applications using DLAS has expanded significantly owing to its potential to characterize flows in many types of ground test facilities [1]. From a gas dynamic standpoint, the DLAS technique saw early use in shock-tube studies [2]. During the first half of the 1990s scramjet propulsion diagnostics were being done with DLAS in the NASA Ames Research Center 16 in. Shock-Tunnel Facility to monitor combustion species [3]. In the mid-to-late 1990s the DLAS technique was used in the ONERA F4 Hot Shot Tunnel [4,5] and the DLR piston-driven shock-tunnel HEG [6] facilities to characterize the nonequilibrium freestream via NO, H_2O, and CO absorption. From these applications it was determined that more measured data, especially vibrational temperatures, are needed for model validation, but the DLAS technique was proving itself. Concurrent efforts to characterize hypervelocity facilities were reported by the Stanford High Temperature Gasdynamics Laboratory (HTGL) group in cooperation with CUBRC to develop a workable sensor to probe H_2O transitions in the LENS-I facility [7]. Plasma facility diagnostics have also been performed using DLAS in the NASA Ames Research Center IHF (60 MW) arcjet facility by the HTGL group to probe high-energy metastable states of O and N [8].

More recent work in hypervelocity facility freestream characterization involved the development of a sensor to probe NO in the CUBRC 48-inch Tunnel and LENS-I Facility based on quantum cascade laser (QCL) technology to probe deeper in the infrared (IR) (about 5500 nm) where stronger NO transitions reside [9]. Also, efforts recently have begun to characterize hypersonic wind tunnels simulating high enthalpy CO/CO_2 flows for Martian atmosphere entry testing [10,]. This DLAS work has shown several instances of numerical simulations not appropriately accounting for nonequilibrium effects in hypersonic ground testing. This has led to DLAS being added to a list of significant methods in nonintrusive diagnostics [11].

Using a tunable diode laser to scan an absorption feature, an absorption line can be measured and exploited by relating linecenter frequency shift to velocity, linewidth to translational temperature, and integrated area to pressure. The objective of the present work is to extend the application range of DLAS by developing a sensor to measure freestream test conditions for hypervelocity CO_2 flows in the VKI Longshot Facility. This paper begins with a description of the Longshot facility and a discussion of the facility CO_2 test condition used for the sensor design. The test conditions were used to design the sensor and to simulate its performance including an analysis of likely flow property gradients. This design study is followed by a description of the arrangement of all sensor components. A discussion of bench qualification results follows the design study. Finally, concluding remarks are given about the sensor and its ability to potentially probe the Longshot freestream.

II. Longshot Facility

The Longshot is a free-piston gun tunnel hypervelocity facility (see Fig. 1) used for experimental investigations of atmospheric hypersonic flight [12,13]. A driver section is filled to high pressure and is separated from the driven section by an aluminum shear plate, which supports the piston. The driven section is kept at an intermediate pressure between the driver section and the evacuated nozzle and test section separated by a second diaphragm. Test gases in the test section can either be N_2 or CO_2 [14]. The piston is released when excess nitrogen is bled from the circumference of a supporting shear plate. The piston then travels down the 27 m long tube compressing the driven test gas into the reservoir where peak conditions can reach 4000 bar and 2500 K leading to the second diaphragm rupturing. The reservoir gas is then fed through a convergent divergent nozzle accelerating the gas into the test cabin. Nozzle choices include a 42 cm diameter contoured nozzle and two conical nozzles with diameters of 36 and 60 cm. The freestream velocity reaches between 2.0 and 2.5 km/s depending on the test condition. The freestream static conditions are quite cold and at relatively low pressure with initial values around 150 K and several hundred Pa. Test times are normally between 20 and 30 ms. Flow Mach numbers range from 11 to 20 with unit Reynold's numbers

Received 8 February 2010; revision received 8 December 2010; accepted for publication 8 December 2010.

*Currently, Postdoctoral Researcher, Mechanical Engineering, University of Vermont, Burlington, Vermont 05405. Member AIAA.

†Currently, Professor, Mechanical Engineering, University of Vermont, Burlington, Vermont 05405. Associate Fellow AIAA.

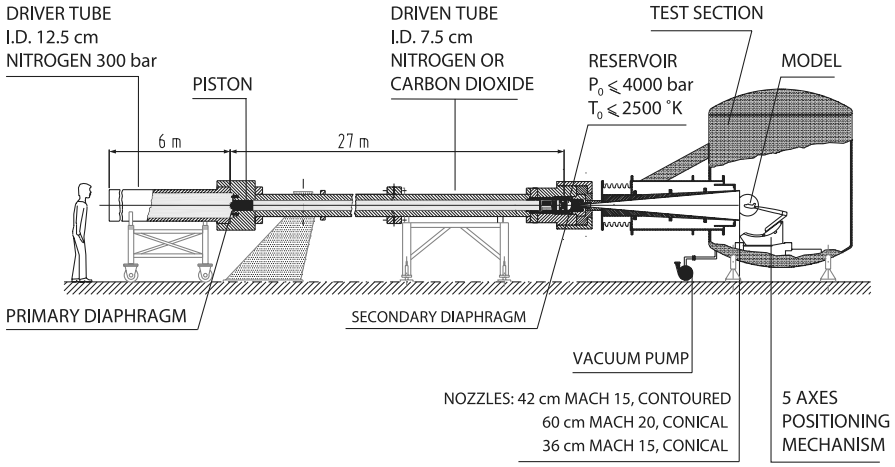

Fig. 1 Longshot impulse hypervelocity facility.

normally between 4×10^6 m^{-1} and 8×10^6 m^{-1} depending on nozzle and test gas choices.

Three parameters are measured with transducers to rebuild the freestream conditions: the reservoir pressure P_0, the total pressure in the test section P_{t2}, and the heat flux to a probe in the test section q_{w2}. Test section values of P_{t2} and q_{w2} are measured on a 2.54 cm hemisphere probe. Using a simple expansion flow model and a Fay Riddell correlation [15] for the test gas starting from P_0 and a guessed total temperature, T_0, the test section values of P_{t2} and q_{w2} are calculated varying T_0 until converged.

Concerns with the current method used to calculate freestream conditions in the Longshot provide additional motivation to incorporate a nonintrusive diagnostics technique to directly probe freestream conditions[‡] [16,17]. While a sensor for N_2 would be most useful, no ro-vibrational bands exist for homonuclear diatomics with a lack of dipole moment. However, it is possible to exploit the ro-vibrational spectrum of CO_2 in the NIR where a number of tunable laser systems are available. Therefore, CO_2 was chosen as the target species for DLAS sensor development for Longshot.

III. Sensor Design Test Conditions

While previous CO_2 testing in Longshot had been conducted using the conical nozzle, ongoing contract testing required use of the isentropically contoured nozzle that was designed for N_2 operation. Development of the sensor for CO_2 flows thus required the definition of a reference CO_2 test condition for the contoured nozzle. Previous conical nozzle tests were used to define this new test condition set with a nitrogen driver pressure of 34.5 MPa, a CO_2 driven pressure of 144 kPa and a piston weight of 1.6 kg.[§] A pressure rake survey was undertaken to assess flow uniformity. Impact pressure results from this test are shown in Fig. 2 showing acceptable flow uniformity in the central core spanning 60% of the exit freejet diameter. The value P_t/P_0 represents the pitot total pressure and reservoir stagnation pressure ratio, which indicates relative uniform Mach number distribution across the core flow.

The reservoir conditions acquired from the data reconstruction typically peak at around 130 MPa and 2700 K. These reservoir gas conditions are rapidly expanded to the freestream conditions. Test time is defined as the period between the initial shock arrival and the unstart process which is typically 20 msec. During this period, the freestream pressure and temperature values will drop from 350 to 100 Pa and 150 to 75 K owing to the constant volume expansion process. A summary of the typical CO_2 Longshot test conditions with the contoured nozzle and rebuilt freestream data for DLAS sensor design are summarized in Table 1.

[‡]Private communication with L. Wolpot, ESA-ESTEC [September 2008].

[§]Private communication with Sebastian Paris, von Kármán Institute for Fluid Dynamics [January 2008].

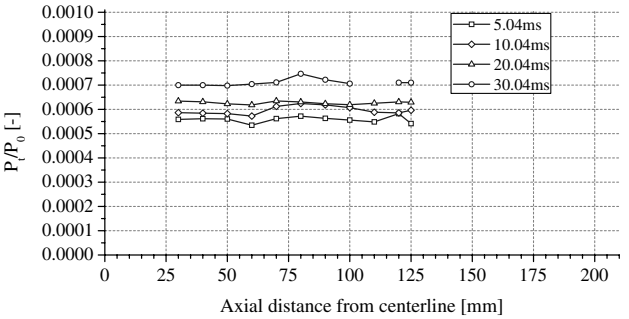

Fig. 2 Impact pressure rake data in freestream showing flow uniformity for the test case with CO_2 test gas and the contoured nozzle. The nozzle wall is located 210 mm away from the centerline.

IV. Transition Selection

The line transition strength $S(T)$ and location ν_0, are important first-step design considerations for DLAS sensor development. There are four potential candidate regions for $^{16}C^{12}O_2$ absorption (which will hereafter be denoted as CO_2) in the NIR at 6250 cm^{-1} (1.6 μm), 5000 cm^{-1} (2.0 μm), 3700 cm^{-1} (2.7 μm) and 2350 cm^{-1} (4.25 μm) as illustrated in Fig. 3, which presents reference ro-vibrational spectra from the HITRAN2004 database [18] for CO_2 and H_2O. Both species should be considered for CO_2 testing where atmospheric humidity may be an issue. It is well understood that transitions in the deeper infrared are stronger, but working deeper in the infrared has drawbacks that will be addressed below along with sensitivity considerations for flow property measurements.

A. Design Consideration: Doppler Shift

The resulting Doppler shifted frequency from a molecule traveling at velocity, u_{gas}, through laser radiation is denoted as $\Delta\nu_{\text{shift}}$. In the Longshot, the angle representing the direction of the light will actually be measured from the flow perpendicular θ. The Doppler shift value as a function of θ then becomes:

Table 1 Typical CO_2 Longshot test conditions with contoured nozzle and extracted freestream data for DLAS sensor design range. Driver gas is N_2 and driven gas is CO_2

P_{driver}, MPa	34.5	P_∞, torr	3–0.75
P_{driven}, kPa	144	T_∞, K	125–75
m_{piston}, kg	1.58 ± 0.01	u_∞, m/sec	2000–1400
P_0, MPa	125 to 15	ρ_∞, kg/m^3	0.02–0.01
T_0, K	2400 to 1200	M_∞	11–10
h_0, MJ/kg	2.0 to 1.0	Re, 1E6/m	6–3
t_{run}, msec	20		

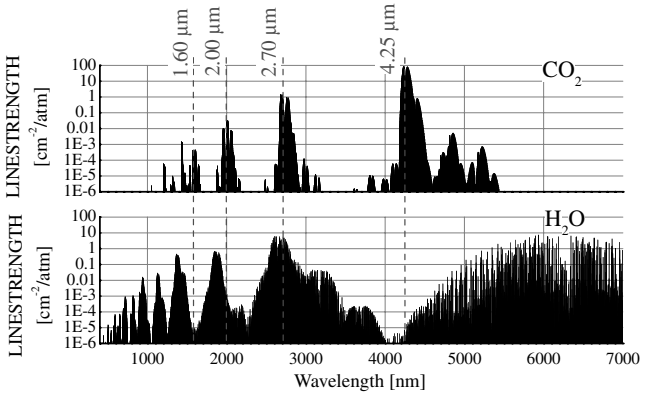

Fig. 3 Ro-vibrational spectra at 300 K of some common species from the HITRAN2004 database.

$$\Delta\nu_{\text{shift}} = \nu_0 \frac{u_{\text{gas}}}{c} \sin(\theta) \tag{1}$$

The line center value ν_0, plays a large role in the Doppler shift magnitude. Deeper infrared transitions lower Doppler shifts which decreases the velocity measurement accuracy, thereby requiring larger angles that may lead to larger probe volumes. Figure 4 illustrates the Doppler shift values for the four band frequencies of interest for CO_2. In terms of providing larger Doppler shift, the more abundant and cheaper laser systems around 6250 and 5000 cm^{-1} perform better. For Longshot, space is limited by the model support system and the fact that the nozzle actually moves a few centimeters during the test. The feasibility range on Fig. 4 illustrates the practical range of configuration angles based on optical access.

B. Design Consideration: Doppler Broadening Sensitivity

The following equation is the common relation for the Doppler width of a spectrally broadened line owing to an assumed Maxwellian thermal velocity distribution of the gas:

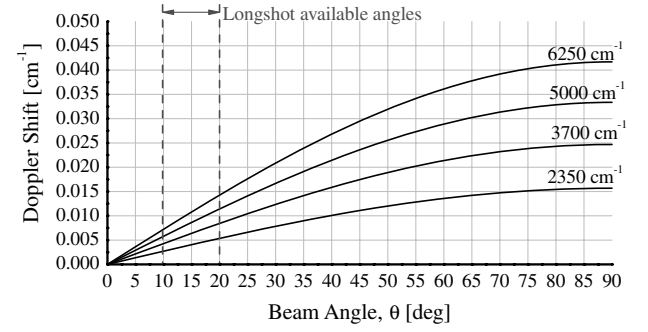

Fig. 4 Doppler shift magnitudes as a function of angle for four CO_2 transition regions.

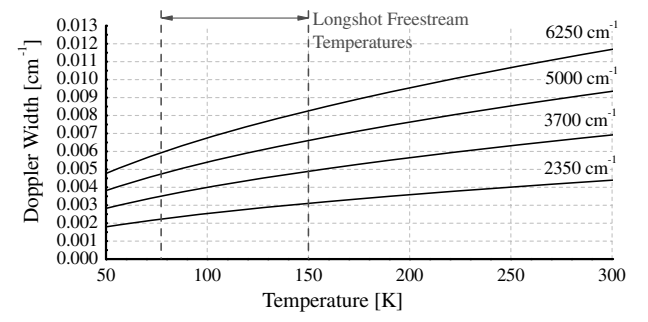

Fig. 5 Doppler width magnitudes as a function of temperature for four CO_2 transition regions.

$$\Delta\nu_D = \nu_0 \left(\frac{8k_B T \ell_n 2}{mc^2} \right)^{\frac{1}{2}} \tag{2}$$

By measuring $\Delta\nu_D$ with all other parameters known (Boltzmann constant k_B, molecular mass m, speed of light c, and linecenter of transition ν_0), we can solve the above expression for the translational temperature. Figure 5 illustrates the Doppler width between 50 and 300 K for the four wavelength regions of interest with sensitivities to temperature illustrated in Fig. 6. Going deeper into the IR reduces both the Doppler width and sensitivity for the same temperature owing to ν_0. Taking only the Doppler width magnitude and sensitivity to temperature factors into account, the 6250 cm^{-1} (1.6 μm) region is better suited for Longshot freestream measurement applications.

C. Laser Selection

A laser system near 1.6 μm (6250 cm^{-1}) was chosen. Lower relative cost, availability of optical components, and the relative water-free range over that of the 2.0, 2.7 and 4.25 μm regions along with the factors described above guided the decision. The main ro-vibrational band of interest near 1.6 μm is the (30013) $\leftarrow$ (00001) "cold" combination band as designated by the Air Force Geophysics Laboratory (AFGL) notation common to the HITRAN database [19]. This band in Herzberg notation is identified as $3\nu_1 + \nu_3$.

We note that while others have used transitions in this region for high temperature combustion applications [20], the low-temperature and low-pressure target conditions for the present work are very different. It is also noted that DLAS probing of CO_2 for Mars atmosphere applications at around 200 K and 6 torr have been performed at 1877 nm [21]. Those tests were time averaged and performed over a longer pathlength to get stronger absorption with higher signal to noise (both of which were not an option for Longshot testing).

A New Focus external cavity diode laser (ECDL) was chosen for turn-key off the shelf operation and excellent narrow linewidth capability (<300 kHz). Usable ranges of the system are on the order of a few hundred wavenumbers. The TLB-6031 model selected incorporates most of the (30013) $\leftarrow$ (00001) combination band which is the strongest band in the 1.6 μm region. However, the laser must be factory set to a narrow tuning range of about 1.5 cm^{-1} to 2.0 cm^{-1} allowing coverage of only one significant ro-vibrational transition in this region.

For spectral model and data reduction purposes, HITRAN 2004 reference linestrength data, $S(T_{\text{ref}})$, were used to estimate linestrengths for Longshot conditions via Eq. (3). Owing to the NIR and the relative low-temperature operation, the fractional term taking into account stimulated emission was neglected as $1 - \exp(-c_2\nu/T) \approx 1$ (where c_2 is the second radiation constant, hc/k_B, and h is Planck's constant). This relation still requires knowledge of reference linestrength and lower-state energy, E'', along with an appropriate model for the total internal partition sum, Q_{int}, at reference and scaled temperatures, T_{ref} and T, respectively.

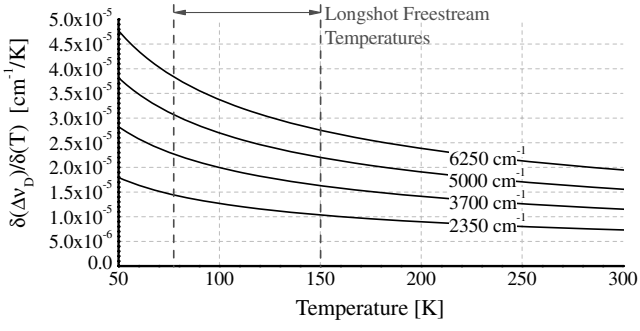

Fig. 6 Doppler width sensitivity to temperature for four CO_2 transition regions.

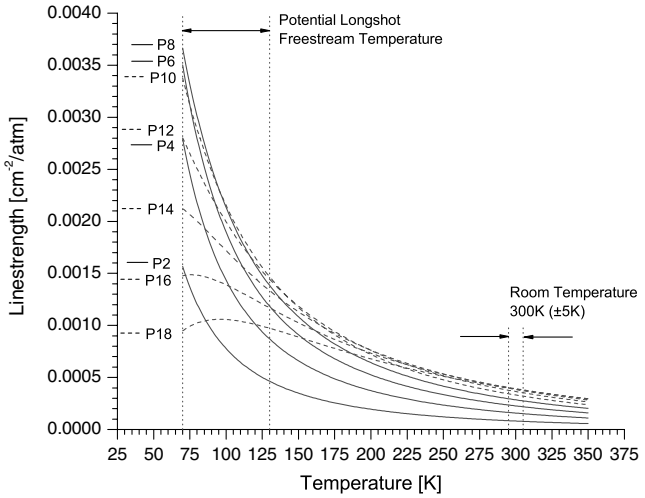

Fig. 7 Linestrength sensitivity to temperature for the P-branch (30013) ← (00001) transitions.

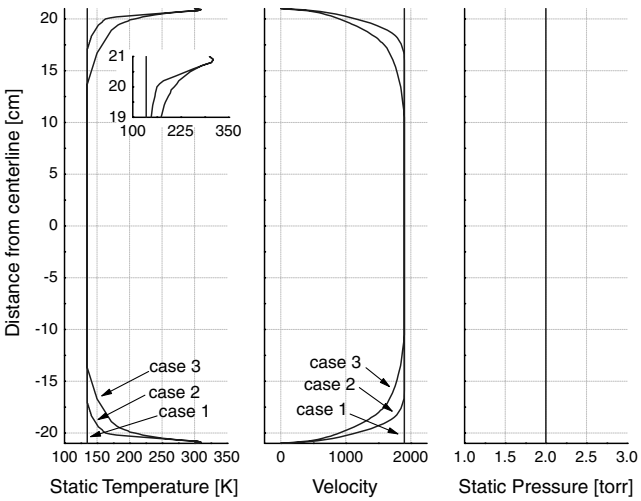

Fig. 8 Theoretical profiles at the nozzle exit plane used for shear layer absorption simulation analysis.

$$S_i(T) = S_i(T_{\text{ref}}) \frac{Q_{\text{int}}(T_{\text{ref}})}{Q_{\text{int}}(T)} \frac{\exp\left(\frac{-c_2 E_i''}{T}\right)}{\exp\left(\frac{-c_2 E_i''}{T_{\text{ref}}}\right)} \tag{3}$$

A third-order polynomial fit was made on a segment of the HITRAN2004 supplied partition sum data from 70 to 300 K to acquire a partition function model for simulation and data reduction purposes valid at room-temperature and Longshot conditions:

$$Q_{\text{int}}(T) = -2.96501 + (0.98321)T + (-8.97249 \times 10^{-4})T^2 + (2.98804 \times 10^{-6})T^3 \tag{4}$$

Given the narrow tuning range, a single ro-vibrational transition must be properly selected to effectively exploit the thermodynamic conditions in the freejet of the Longshot. It is also desirable to have a transition that is a strong absorber in the core flow, but relatively transparent in the higher temperature shear layer. Figure 7 is a plot of the P-branch transitions of the (30013) ← (00001) ro-vibrational band up to a rotational quantum number of 18.

Owing to its strength and temperature dependence, the P12 transition at 6218.09 cm^{-1} was selected for this application. This transition is a strong absorber in the expected freejet core temperatures and relatively weak absorber in the closer to room temperature shear layer. The laser frequency was thus chosen to be centered on 1608 nm (6219 cm^{-1}) with a tuning range of 1607.96–1608.41 nm (6219.06–6217.32 cm^{-1}). Table 2 lists all the CO_2 transitions within the laser tuning range that are cataloged in the HITRAN2004 database including upper-state local quanta q'' and self-broadening coefficients γ_{self}. There is no significant H_2O transition in this range. Analysis of the shear layer absorption for this transition will be presented in the next section.

V. Shear Layer Absorption Analysis

A major challenge for DLAS is dealing with appropriate fitting of absorption profiles where there are property gradients along the line-of-sight over the absorbing pathlength, L. As with all hypervelocity facilities, a boundary layer grows inside the nozzle that ultimately becomes a free shear layer with temperature and velocity gradients between the core flow and the near-evacuated conditions in the test cabin. The goal was to see if target inviscid core temperature and pressure (135 K and 2 torr) can be extracted while absorbing along paths with such shear layer gradients. Cases with a beam perpendicular to the flow and a beam angled 19° from the perpendicular to flow (an expected measurement orientation) were analyzed. Three theoretical profiles were assumed at the nozzle exit with a constant static pressure profile of 2 torr. Figure 8 illustrates these three theoretical cases of temperature and velocity distribution across the freejet with typical reduced freestream values in the inviscid core. Case 1 represents an assumed constant temperature (135 K) and velocity (1900 m/s) without shear layer. Cases 2 and 3 represent increasingly more significant shear layer gradients approaching a zero-velocity room-temperature nozzle wall.

Table 2 CO_2 transitions in laser tuning range

T, K	ν_0, cm^{-1}	S, cm^{-2}/atm	q'	γ_{self}, cm^{-1} atm
296	6217.51	8.349E-06	R30	0.0869
296	**6218.09**	**3.749E−04**	**P12**	**0.1067**
296	6218.29	6.400E − 06	R33	0.0843
296	6218.69	7.010E − 06	R32	0.0852
296	6218.85	3.556E − 06	P26	0.0916

Step 1 was to simulate the total absorption across the integrated path of the freejet using a discretized summation of the form:

$$\int_0^L \alpha(\nu, P, T)\, \mathbf{d}x = \int_0^L PS(T)\phi_V(\nu, P, T)\, \mathbf{d}x \tag{5}$$

$$\alpha(\nu, P, T)L = \sum P_j S(T_j)\phi_V(\nu, P_j, T_j)\Delta x_j \tag{6}$$

At each discretized step a temperature and pressure dependent Voigt model [22], $\phi_V(\nu, P_j, T_j)$, was used to represent the lineshape, ϕ_V, which depends on both temperature and pressure through the collisional and thermal broadening mechanisms. Reference self-broadening width was taken from HITRAN2004 and the collisional broadening exponent n was assumed to be 0.7 as it was felt the dispersion interaction was more realistic than the hard sphere model. For the angled beam case, each discretized step was shifted by the appropriate Doppler shift according to the local gas velocity. The line strength was scaled via the relation in Eq. (3) for the appropriate temperature at the discretized point.

Step 2 was to fit the simulated data from Step 1 using a similar Voigt model but dependent on the Doppler and collisional half-widths, $\phi_V(\nu, \Delta\nu_C, \Delta\nu_D)$, while assuming constant flow properties along the absorbing path. The resulting Doppler width contribution to the Voigt fit was used to extract the temperature. Pressure was then acquired from the integrated area of the absorption fit. All simulated integrated-path absorption cases without the angled beam (case 1, case 2, and case 3) have profiles with no noticeable asymmetry and are quite accurately fit. In the angled beam cases 2 and 3, there is only a slight asymmetry in the simulated spectrum. This owes to the choice of the P12 (30013) ← (00001) transition being investigated for this testing campaign in which the linestrength is about a factor of

Table 3 Fitting results to simulated data with shear layer influence. Target core flow temperature and pressure to be extracted are 135 K and 2 torr, respectively

Transition	Test case	T, K	P, torr
P12	1	135	1.99
P12	2	136	1.94
P12	2 at 19°	134	1.90
P12	3	139	1.91
P12	3 at 19°	137	1.86
P18	3 at 19°	**109**	**1.33**

4 stronger at the core temperature conditions than at the shear layer temperature conditions.

Table 3 lists the temperature and pressure values derived from the fit results for these various temperature/velocity profile and angle beam tests. This analysis shows that the use of a Voigt profile over the entire freejet absorbing path will not lead to significant misinterpretations of the core temperature owing to shear layer absorption for P12 transition. This is not the case for the P18 transition whose shear layer sensitivity is stronger. However, pressure extraction may become more challenging further into the test as the shear layer grows while the test cabin pressure increases and reservoir pressure decreases. This represents a challenge for defining an appropriate path length for extracting species density and pressure.

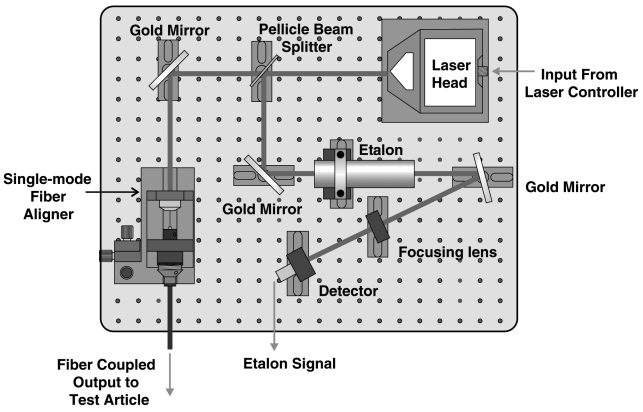

Fig. 9 DLAS portable bench illustration.

VI. Sensor Arrangement

The sensor was developed onto a portable bench with fiber optic integration to facilitate porting the experiment from absorption cell to facility and vice versa (Fig. 9). The varying frequency output of the laser (via piezo voltage) was directed to a pellicle beam splitter with an 8% total reflection. The 8% reflected light was steered to pass through an air-gapped etalon for frequency marking with a free spectral range of 1.583 GHz at 1600 nm. The light after the etalon was directed to a Thorlabs DET410 high-speed photodetector. The light that passed through the pellicle beam splitter I_0 was steered toward the single-mode fiber coupler for free-space to fiber coupling. This fiber coupled light was then directed by a secondary fiber through an absorbing medium with the transmission signal I being recorded by a second photodetector.

Reference intensities can be extracted using a baseline fitting method illustrated in Fig. 10. This figure illustrates a transmitted signal with two absorption features being recorded which are trimmed to exclude the absorption feature and other contaminants to an ideal baseline fit (plots A and B). Those points without absorption are then fitted with an appropriate model (plot C). This fit represents the reference intensity I_0, and is used to calculate absorption via $-\ln(I/I_0)$ (plot D).

This approach can relieve some issues such as the fact that a measured reference signal does not take into account the effects of the interference from optical windows or other absorbing media that would be present in the transmitted signal. Other benefits include the simplification of the experimental setup by freeing up one channel of data acquisition as well as reducing the amount of optics and detectors required for the experiment. For certain conditions, i.e., narrow absorption features, a sufficient baseline fit can be made with little loss in accuracy when compared with using a reference signal as a baseline.

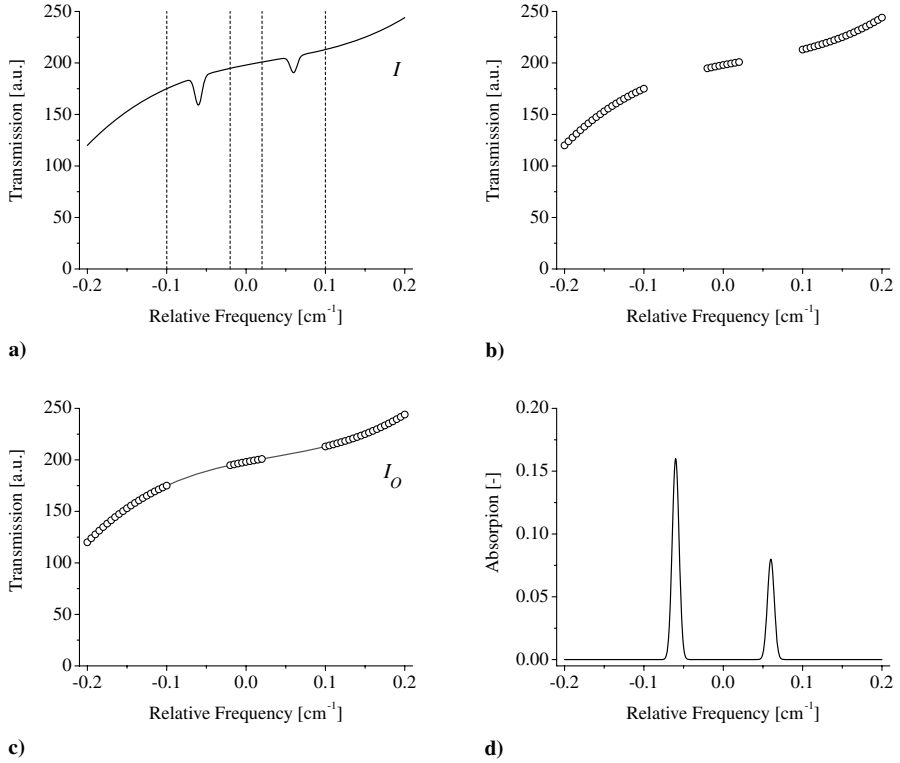

Fig. 10 Two-peak data reduction illustration using baseline fitting technique with absorption in plot D calculated via $-\ln(I/I_0)$.

VII. Bench Tests

The primary direct absorption calibration tests used a flowing absorption cell capable of maintaining subtorr pressures in a pure gas environment. The light was delivered from the portable laser bench by a 5 m long APC single-mode fiber. The light was collimated to about 4 mm in diameter and directed through the flow reactor. The absorption cell had Brewster angled windows which helped reduce etaloning. This was set up into a double pass configuration giving a total pathlength of 56 cm. The 4 mm diameter collimated transmitted light had a divergence of approximately 0.05° and was focused onto a 5 mm diameter active region fast response DET50 model photodetector using a 25 mm diameter lens with a 150 mm focal length. It was assumed that all the transmitted light was being collected onto the detector for the bench tests. This larger active region was chosen to limit the influence of mechanical vibrations during Longshot runs. Data acquisition was done with a 16-bit National Instruments card with simultaneous sampling at 800 kS/sec for each of the four available channels. The detector is terminated into 50 Ω to maximize bandwidth. While the ECDL can be driven to several kHz via the piezo-mechanical drive, a modest 300 Hz (two scans per period yielding a 600 Hz scan rate) sine wave drove the laser. The use of a linear saw-tooth tuning waveform instead of a sinusoidal one would eliminate one nonlinearity, but at this tuning frequency unacceptable jitter was observed in the transmission signal at the turnaround points. Temperature and current tuning would eliminate the jitter problem as well, but the tuning current/temperature depth for our system was not sufficient to cover the absorption feature. The scan rate was chosen as a tradeoff between acquiring enough data points per scan with DAQ sampling resolution and generating enough scans per test in the 20 ms run duration. Single scan duration at 600 Hz is 1.6 ms with less than 10% of the scan containing the absorption feature. This implies there is essentially a flow time average of approximately 160 μs. DAQ sampling of 800 kS/sec per channel yields a time between data points of 1.250 μs which is more than twice the detector rise time of 0.439 μs producing 100+ samples covering the absorption feature.

Figure 11 illustrates how a transfer function is derived from a typical etalon trace. The top plot represents a single etalon scan from one of the bench tests with detected peaks superimposed. These peaks were separated equally in frequency space with the free spectral range (FSR) value of 0.0528 cm^{-1}. The bottom plot represents these peak time instances plotted as steps in the etalon FSR value. This data was then fit with a third-order polynomial to give a transfer function equation specific to this scan in relative frequency.

Seven pressure cases (4.5, 14.2, 26.2, 47.2, 76.1, 97.0, and 119.0 torr) were tested for this bench campaign. For each case, the transmission data in wavenumbers had been separated and trimmed into a compact single scan. This trimming entails the removal of end noise jitter and laser turnaround influence on the smooth signal. Absorption was extracted for each individual scan via the method illustrated in Fig. 10. Figure 12 represents the transmission and baseline fitting data of two test pressure cases; 4.5 and 119 torr. The 4.5 torr provides the closest match to Longshot freestream absorption characteristics in terms of low absorption level and Doppler to collisional width ratio.

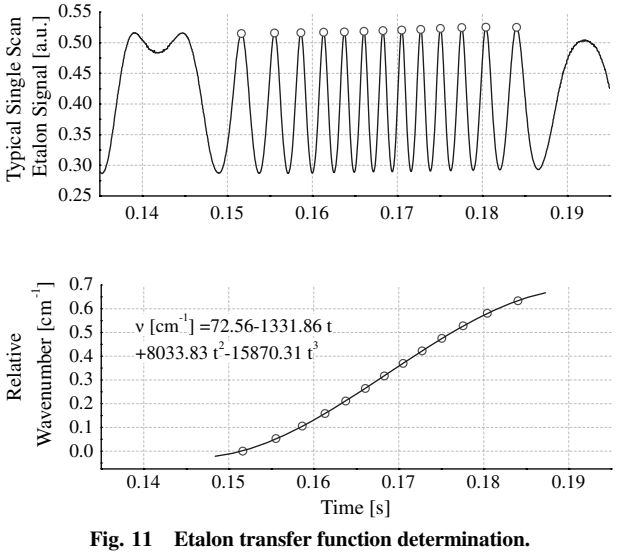

Fig. 11 Etalon transfer function determination.

Although the tuning range of the laser is about 1.7 cm^{-1}, tuning nonlinearities limit the useful scan to about 0.6–1.25 cm^{-1}. These nonlinearities come from the sine wave tuning, the optics incorporated, and the power tuning characteristics of the laser and generate several inflection points through the tuning range of the laser. Nothing can be done about the sine wave tuning or the power tuning characteristics of the laser but wedged and angled optics can reduce the optical component influence. Baseline nonlinearities encountered with DLAS sensors are normally not an issue when absorption levels are significantly higher (over 20%). However, as the absorption levels in Longshot are expected to be between 1 and 2%, these influences needed to be addressed with more attention. When the optical nonlinearities are minimized, the P12 absorption feature lies well away from baseline inflection points at low pressures, as seen in the 4.5 torr case of Fig. 12. However, as pressure increases, the profile width and thus the tuning range must be increased to acquire sufficient baseline information. Unfortunately, this adds more transmission nonlinearities to the baseline signal effecting the ability to extract accurate absorption. This is evident in the 119 torr case of Fig. 12. It was determined that for over 50 torr the baseline data were too few for an adequate baseline fit for the tuning range of the laser.

The data extraction process began with the analysis of the baseline signal. The baseline polynomial order was adjusted until the baseline absorption signal is zero without any negative values. The chosen baseline also needs to yield a low residual between experiment and Voigt fit data. When done properly there was a convergence of near room temperature and cell pressure. This is considered to be the optimal fit for reduction. A Doppler and collisional width dependent Voigt fit was then used to extract the gas temperature from the Doppler width contribution. A study of collisional width temperature dependence (from $n = 0.5$ to $n = 0.7$) showed no change in temperature values determined from the width dependent Voigt model. We attribute this to the fact that $\Delta\nu_D \gg \Delta\nu_C$ for low-pressure

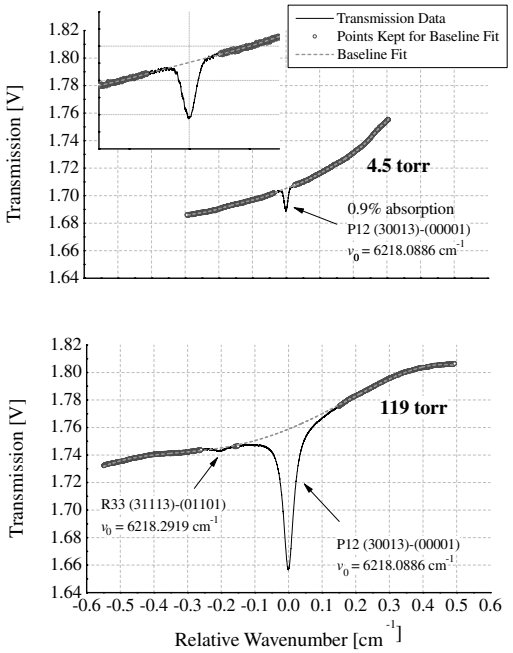

Fig. 12 Baseline extraction comparison two different pressure cases. Inset plot represents zoomed-in portion of 4.5 torr absorption feature illustrating signal quality at 0.9% absorption.

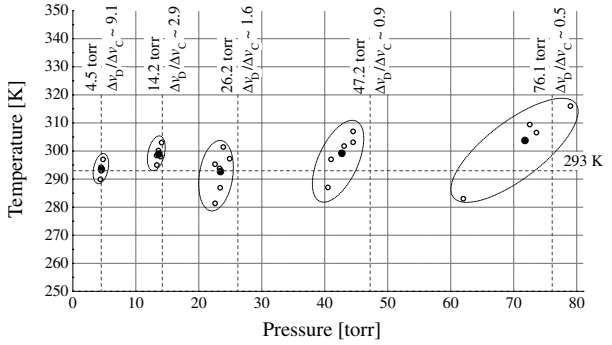

Fig. 13 Extracted temperature and pressure from bench tests for narrow tuning over absorption feature. Temperature was extracted from the Doppler FWHM contribution to the Voigt fit with pressure coming from feature integrated area.

sensor development and application conditions. Recall that for the 4 torr case, $\Delta\nu_D/\Delta\nu_C$ quite close to the ratio we expect for the Longshot freestream conditions. Linestrength was calculated from the extracted temperature and used along with the absorption pathlength and integrated area to determine pressure.

Figure 13 shows the extracted temperature and pressure from these tests. The vertical dashed lines indicate the pressure reading from the cell Baratron transducer. These tests show that at low pressure reasonable agreement exists. However, as the pressure is increased above 50 torr, significant deviation appears. This is evident as the band of data for each test condition (represented in the dashed ellipses) tends to grow larger and larger as pressure increases. Decreasing $\Delta\nu_D/\Delta\nu_C$ with increasing pressure as well as error in interpreting an appropriate baseline are the primary causes of this. Stronger absorption through longer pathlength would help to reduce the baseline issues. A Heriot-type multipass cell would be ideal for low-pressure spectra measurements on the bench but a detectability of 0.9% direct absorption (4.5 torr case) over signal noise is clearly feasible with this configuration which is important as single-pass Longshot absorption levels for this system are expected to be between 1 and 2%. Moreover, the potential for extracting useful temperature and pressure information at low pressure is evident. Thus, it should be possible to extract a baseline for Longshot freestream conditions in terms of tuning range for an adequate baseline as the features will be quite narrow (around 0.008 cm^{-1}).

Validating the data in frequency space was also of significant importance. The two strongest transitions in the tuning range of the laser are the P12 (30013) ← (00001) transition of primary interest and the R33 (31113) ← (01101) transition. The R33 transition will not be visible in the cold freestream conditions of the Longshot owing to its high rotational quantum number. However, in the flow reactor tests near room temperature it is distinguishable above the signal noise. Thus, it can be used to check the process of changing the absorption scans in time to wavenumber as the line positions of these transitions are quite accurately known. The two-peak Voigt fit in Fig. 14 show ν_0 values with a difference of 0.20357 cm^{-1} between them. The HITRAN2004 values of 6218.2919 cm^{-1} for the R33 transition and the 6218.08855 cm^{-1} for the P12 transition give a difference of 0.20335 cm^{-1}. A total difference between the two-peak separation values is only 0.00022 cm^{-1} which is only a 0.098% difference from the HITRAN value illustrating that the transfer function method with the etalon was performing well within the available HITRAN database error ranges.

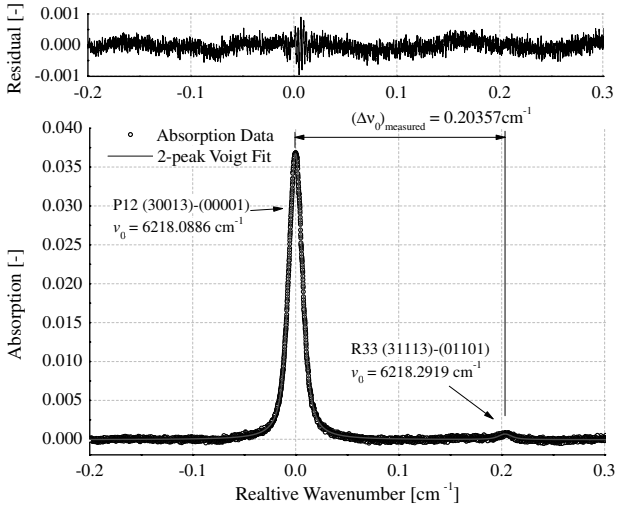

Fig. 14 Fitting of test data in the flow reactor at 26 torr.

VIII. Conclusions

This article details the development of a DLAS sensor for probing the freestream conditions for CO_2 flows in a high Mach number and high Reynold's number impulse flow environment (VKI Longshot facility). A CO_2 ro-vibrational transition near 1600 nm was chosen as measured parameter sensitivity issues outweighed absorption strength benefits deeper in the infrared. The selected target P12 (30013) ← (00001) transition was analyzed for shear layer absorption effects. This analysis showed that the effects of property gradients along the freejet absorbing path can be greatly reduced if a proper transition, such as P12 for these conditions, is selected. A portable optics bench was built to facilitate moving the system from bench test to facility and vice versa.

The motivations for performing the simulation and bench tests were to develop confidence in the equipment, verify the spectral models used and to ensure that bench tests at conditions close to Longshot freestream values meet expectations. The use of a 800 kS/ sec per channel, 16-bit DAQ system provide the ability to capture adequate data points and detect 1–2% absorption with very good signal to noise even for the 600 Hz scan rates needed for Longshot testing. More important, these tests showed good performance at $\Delta\nu_D/\Delta\nu_C$ levels expected in the Longshot freestream.

Acknowledgments

This work has been supported by the U.S. Air Force Office of Scientific Research (Grant FA9550-07-1-0089, J. Schmisseur, Technical Monitor), the Centre National d'Etudes Spatiales (MSRO-052, J.-M. Charbonnier, Technical Monitor), and the Belgian American Educational Foundation (Emile L. Boulpaep).

References

[1] Hanson, R. K., and Jeffries, J. B., "Diode Laser Sensor for Ground Testing," *25th Ground Testing Conference*, AIAA Paper 2006-3441, July 2006.

[2] Hanson, R. K., "Shock Tube Spectroscopy: Advanced Instrumentation with a Tunable Diode Laser," *Applied Optics*, Vol. 16, 1977, p. 1479. doi:10.1364/AO.16.001479

[3] Newfield, M. E., Loomis, M. P., Gopaul, N. K. J. M., Ghorbani, A., Kowalski, T. R., and Cavolowsky, J. A., "Optical Fiber Applications of Laser Absorption Diagnostics in Scramjet Combustors," *32nd Aerospace Sciences Meeting*, AIAA Paper 94-0386, Jan. 1994.

[4] Mohamed, A., Rosier, B., Henry, D., Louvet, Y., and Varghese, P. L., "Tunable Diode Laser Measurements on Nitric Oxide in a Hypersonic Wind Tunnel," *AIAA Journal*, Vol. 34, No. 3, March 1996, pp. 494–499. doi:10.2514/3.13095

[5] Sagnier, Ph., Vrant, J. L., Devezeaux, D., Mohamed, A. K., and Masson, A., "Real Gas Flow Characterization in the ONERA F4 High Enthalpy Wind Tunnel," ONERA BP 72 92322, Chatillon, France, 1997.

[6] Mohamed, A.-K., Henry, D., Falni, J.-P., Sagnier, P., Soutad, J., Beck, W. H., and Martinez Schramm, J., "Infrared Diode Laser Absorption Spectroscopy Measurements in the S4MA, F4 and HEG Hypersonic Flows," *International Symposium on Atmospheric Reentry Vehicles and Systems*, ONERA Paper No. TP 1999-45, March 1999.

[7] Wehe, S. D., Baer, D. S., and Hanson, R. K., "Measurement of Gas Temperature and Velocity in Hypervelocity Flows using a Diode-Laser Absorption Sensor," *20th AIAA Advanced Measurement and Ground Testing Conference*, AIAA Paper 98-2699, 1998.

[8] Kim, S., Jeffries, J. B., Hanson, R. K., and Raiche, G. A., "Gas Temperature in the Arc-Heater of a Large Scale Arcjet Facility Using Tunable Diode Laser Absorption," *43rd Aerospace Sciences Meeting*, AIAA Paper 2005-900, 2005.

[9] Parker, R. A., Wakeman, T., MacLean, M., and Holden, M., "Measuring Nitric Oxide Freestream Concentration Using Quantum Cascade Lasers at CUBRC," *44th AIAA Aerospace Sciences Meeting and Exhibit*, AIAA Paper 2006-926, Jan. 2006.

[10] Mohamed, A., Verant, J. L., Soutad, J., Viguier, P., Van Ootegem, B., and Tran, P., "Mid-Infrared Diode Laser Absorption Spectroscopy Measurements in CO/CO_2 Hypersonic Flows of F4 and SIMOUN," *Sixth European Symposium on Aerothermodynamics for Space Vehicles, Session S22: Measurement Techniques and Instrumentation*, SP-659, ESA, Noordwijk, The Netherlands, Nov. 2008.

[11] Mohamed, A. K., Bonnet, J., Lefebvre, M., Desormeaux, A., Millan, P., Hoonaert, A., and Pot, T., "Development of Optical Techniques at ONERA for Hypersonic Reentry," International Academy of Astronautics, and the International Institute of Space Law, Paper No. IAC-03-V.6.08, Sept.–Oct. 2003.

[12] Backx, E., "The Total Temperature in the Longshot Wind Tunnel : Its Measurement and Evaluation," von Kármán Institute for Fluid Dynamics, Technical Note 98, Rhode-Saint-Genese, Belgium, April 1974.

[13] Simeonides, G., "The VKI Hypersonic Wind Tunnels and Associated Measurement Techniques," von Kármán Institute for Fluid Dynamics, Technical Memorandum 46, Rhode-Saint-Genese, Belgium, Nov. 1990.

[14] Simeonides, G., Paris, S., and Dieudonne, W., "Extensions of the Operating Domain of the VKI Longshot Tunnel to the Use of Testing Gases with Various γ Values 87th Supersonic Tunnel Association, ONERA, VKI RP 1997-40, Modane, France, May 1997.

[15] Fay, J. A., and Riddell, F. R., "Theory of Stagnation Point Heat Transfer in Dissociated Air," *Journal of the Aeronautical Sciences*, Vol. 25, No. 2, Feb. 1958, pp. 73–85.

[16] Fletcher, D. G., "Recommended Real Gas Equation of State for CO_2 Testing in Longshot," von Kármán Institute for Fluid Dynamics, Contract Rept. MARS-TN-MSRO-019-VKI, 2003.

[17] Laurent, S., "Numerical Simulation of CO_2 in Hypersonic Wind Tunnels and in Atmospheric Reentry Conditions," von Kármán Institute for Fluid Dynamics, Student Rept. 2003-2004.

[18] Rothman, L. S., Jacquemart, D, Barbe, A., Benner, D., and Birk, M., "The HITRAN 2004 Molecular Spectroscopic Database," *Journal of Quantitative Spectroscopy and Radiative Transfer*, Vol. 96, No. 2, 2005, pp. 139–204. doi:10.1016/j.jqsrt.2004.10.008

[19] Rothman, L. S., and Young, L. D. G., "Infrared Energy Levels and Intensities of Carbon Dioxide-II," *Journal of Quantitative Spectroscopy and Radiative Transfer*, Vol. 25, No. 6, 1981, pp. 505–524. doi:10.1016/0022-4073(81)90026-1

[20] Mihalcea, R. M., Baer, D. S., and Hanson, R. K., "A Diode-Laser Absorption Sensor System for Combustion Emission Measurements," *Measurement Science and Technology*, Vol. 9, No. 3, 1998, pp. 327–338. doi:10.1088/0957-0233/9/3/004

[21] Le Barbu, T., Vinogradov, I., Durry, G., Korablev, O., Chassefière, E., and Bertaux, J. L., "TDLAS: A Laser Diode Sensor for the In-Situ Monitoring of H_2O, CO_2 and Their Isotopes in the Martian Atmosphere," *Advances in Space Research*, Vol. 38, No. 4, 2006, pp. 718–725. doi:10.1016/j.asr.2005.04.049

[22] McLean, A. B., Mitchell, C. E. J., and Swanston, D. M., "Implementation of an Efficient Analytical Approximation to the Voigt Function for Photoemission Lineshape Analysis," *Journal of Electron Spectroscopy and Related Phenomenon*, Vol. 69, 1994, pp. 125–132.